Iranian Journal of Science and Technology, Transactions of Civil Engineering
https://doi.org/10.1007/s40996-023-01061-6

RESEARCH PAPER

Performance of Slag-Pumice-Based Alkali-Activated Mortar at Ambient Environment

Arass Omer Mawlod[1,2] · Dillshad Khdhir Hamad Amen Bzeni[2] · Radhwan Alzeebaree[3,4]

Received: 8 November 2022 / Accepted: 29 January 2023

Abstract

Sustainability in construction materials is a hot topic of research, and alkali-activated materials are believed to be a real alternative to OPC concrete. The manufacturing process of cement emits nearly 8% of CO_2 into the atmosphere. This study utilised slag as a base binder in the alkali-activated mortar (AAM). The pumice powder was used as a replacement ratio of (0, 10, and 20) % by the mass of the slag. Three various ratios of alkali solution-to-binder ratio (s/b) were utilised (0.4, 0.5, and 0.6) for a detailed evaluation of the fresh and hardened properties of alkali-activated mortar. The setting time and flow test were conducted, and the mechanical characteristics were investigated through compressive strength, flexural strength, and direct tensile strength. Furthermore, fire resistance, water absorption, water sorptivity, porosity, density, efflorescence, and sulphate resistance were all examined to evaluate the durability characteristics of AAM. Results showed that increasing the amount of pumice powder in the mixture reduced its flowability for all s/b ratios. At a s/b of 0.4, increasing the pumice powder concentration degraded the mechanical and durability qualities. Simultaneously, increasing the amount of pumice powder at both s/b of 0.5 and 0.6 increased the mechanical and durability properties.

Keywords Direct tensile strength · Fire resistance · Pumice powder · Water sorptivity · Efflorescence · Sulphate attack

Abbreviations

AAM	Alkali-activated mortar
s/b	Solution-to-binder ratio
AAC	Alkali-activated concrete
OPC	Ordinary Portland cement
g	Gram
°C	Degree Celsius
hr	Hour
MPa	Mega pascal
SEM	Scanning electronic microscopy
GGBFS	Ground-granulated blast furnace slag

1 Introduction

Alkali-activated concrete (AAC) is on its way to becoming a reasonable alternative to Portland cement, and extensive research on all components of AAC continues. The unsustainable nature of conventional Portland cement as well as major air pollution concerns are motivating factors behind the development of AAC (Abdollahnejad et al. 2018). Environmental friendliness, low cost and fire resistance are all primary motivators (Davidovits 2008). The building sector is a major consumer of natural resources. Alkali-activated concrete recycles industrial by-products, making it more sustainable than regular Portland cement concrete for a variety of reasons, such as low carbon, environmentally friendly and energy efficient (Abdollahnejad et al. 2018). Complete replacement of ordinary Portland cement by geopolymers reduces 80% of CO_2 emissions than the utilisation of cement (Zhao et al. 2007). Alkali-activated materials are now being studied globally to standardise all components of the new generation of construction materials (Davidovits 2008; Provis 2018; Ameri et al. 2019; Degefu et al. 2022).

Alkali-activated concrete is produced by activating aluminosilicate materials with an alkali solution. Accordingly, they activate materials containing aluminosilicates, such as

✉ Arass Omer Mawlod
arass.omer@uor.edu.krd

1 Civil Engineering Department, University of Raparin, Ranya, Kurdistan Region, Iraq

2 Civil Engineering Department, Salahadin University, Erbil, Kurdistan Region, Iraq

3 Highway and Bridge Department, Duhok Polytechnic University, Duhok, Kurdistan Region, Iraq

4 Civil Engineering Department, Nawroz University, Duhok, Kurdistan Region, Iraq

Published online: 18 February 2023

industrial by-products like silica fume (Xinyan, Yanghai and Liang 2022), fly ash (Antoni et al. 2020), ground-granulated blast furnace slag (Bingöl et al. 2020) and ceramic wastes (Alzeebaree et al. 2021), and natural materials like metakaolin (Chakkor, Altan and Canpolat 2022), rice husk ash (Mahdi et al. 2022), calcined clay and volcanic tuff (Clausi et al. 2018; Zamanabadi et al. 2019; Mawlod 2020; Alzeebaree et al. 2021). The reaction produces a three-dimensional framework with SiO_4 and AlO_5 tetrahedra connected at the corners by shared O atoms, resulting in new silicate aluminate molecules (Davidovits 1991). The chemical reactions are affected by the composition of the base material. The high amorphous alumina and silica concentration of the starting base material increases reactivity. These reactions are called alkali-reactive and have a positive influence on the characteristics of the hardened AAC (Duxson et al. 2007; Provis and Bernal 2014; Mobasher et al. 2016; Kurtoğlu et al. 2018).

Pumice is a white, light, silica-rich volcanic tuff. It is made up of amorphous volcanic tuff with low density (0.5–1 g/cm^3) owing to its porous structure. Therefore, pumice is used as a construction material. In addition, pumice powder is frequently used as a binder material due to its cementitious properties (Kabay et al. 2015). The mineralogy and crystallinity of pumice powder influence its chemical reactivity (Nesbitt and Young 1984). Pumice powder has been used as a construction material in ancient building. It was mixed with lime to produce a durable and strong mortar (Shi and Day 1993; Goldsworthy and Zhu 2009; Allen 2015). Calcium aluminosilicate hydrate C-A-S-H with suitable binding characteristics can be produced by dissolving aluminosilicate materials in lime solution (Jha and Singh 2011; Mason 2012; Nath and Sarker 2015; Walkley et al. 2015; Al-Zboon et al. 2016; Djobo et al. 2016; Tekin 2016; Mawlod 2020).

According to research, the chemical interaction between alkali solution and base material is an endothermic reaction (Mohamed et al. 2019). AACs are limited in their application due to the use of fly ash as a base ingredient and the need for heat for curing (Noushini et al. 2016). The best curing time and temperature were concluded to be 18 h at 75 °C. Therefore, researchers attempt to develop ambient curing with AAC to overcome this limitation (Gülşan et al. 2019; Eren et al. 2021).

According to the researcher, geopolymerisation and hydration yield N-A-SH and C-S-H gels, respectively. These gels outperformed slag-based AAM in terms of compressive strength and sulphate attack (Guerrieri and Sanjayan 2010; Bernal et al. 2012; Yang et al. 2012; van Deventer et al. 2015; Winnefeld et al. 2015; Kurtoglu et al. 2017). Furthermore, some researchers believe that increasing the amount of slag remarkably enhances compressive strength. However, the flowability and setting time were reduced; mixing AAC with a high slag content was found appropriate for ambient curing and application in construction site (El-Hassan and Ismail 2018; Eren et al. 2021). Nis, Eren and Çevik, (2021) investigated fresh and mechanical properties of fibre-reinforced slag-based alkali-activated concrete. Fibre inclusion was concluded to have improved all mechanical properties and decreased the flowability of concrete. Eren et al. (2021) studied the combined effect of steel fibre and crumb rubber on the fresh and mechanical properties of slag-based geopolymer concrete. They concluded that crumb rubber and fibre inclusion negatively affect the workability of the mixes. Furthermore, they reported that increasing the crumb rubber decreased the mechanical properties. Kadhim et al., (2022) studied the fresh and mechanical characteristics of fibre-reinforced slag-based geopolymer mortar at elevated temperature. They concluded that 1% of the PVA fibre addition improved flexural and splitting tensile strength. Raising the temperature to 250 °C shows further improvement, whereas increasing the temperature to 500 °C degraded the mechanical properties. Aljanabi et al., (2022) studied the residual strength of alkali-activated composite. Increasing the temperature from 0 to 250 °C was reported to improve the compressive strength. However, raising the temperature to 500 °C temperatures deteriorated the compressive strength.

Efflorescence is one of the most essential properties of durability. It refers to the formation of a white alkali deposit on the material's surface within the porous structure (Kani et al. 2012). Potassium silicate, heat curing and alumina-rich admixtures can all contribute to the elimination of efflorescence (Pouhet 2015).

Rare or few investigations have been done on the impact of the use of pumice on the behaviour of slag-based alkali-activated mortar (Provis and Bernal 2014). Therefore, this study examines the effect of using pumice on the characteristics of slag-based alkali-activated mortar. Fresh properties were found in terms of setting time and flow test. By contrast, the mechanical properties were investigated through the evaluation of compressive strength, flexural tensile strength and direct tensile strength. The durability properties such as water sorptivity, fire resistance, porosity, water absorption, density, efflorescence and sulphate attack were also studied. Therefore, this investigation is an attempt towards examining the feasibility of utilising sustainable materials in the construction sector, especially for precast concrete items. Furthermore, the ambient-cured slag-based sustainable alkali-activated materials will reduce the limitations of heat-cured AAM on the site application.

2 Experimental Works

2.1 Materials

Ground-granulated blast furnace slag (GGBFS) was utilised as a binder. Pumice stone was also provided and crushed to a powder to achieve the fineness of pumice powder as depicted in Fig. 1. Slag and pumice powders were obtained from a local supplier. Table 1 presents the chemical composition of slag and pumice powders. Locally available river sand was used regarding ASTM C33. Both sodium silicate solution and sodium hydroxide flakes with a purity of 99% were also obtained from local supplier. Sikament-1 N plus which is a naphthalene-based admixture was used to improve the workability of the mixture.

2.2 Mixing, Casting and Curing

Alkali solution was prepared by melting sodium hydroxide flakes in tap water with a concentration of 12 M and mixed with sodium silicate in a ratio of 1:2.5 (Kwek, Awang and Cheah 2021). Binder (slag and pumice powder) and sand were mixed dry in a ratio of 1:1. The alkali solution-to-binder ratios were 0.4, 0.5 and 0.6. The alkali solution was poured onto the dry materials and mixed manually. The mixture was placed in the moulds in two layers and compacted manually. The durability and compressive strength tests were carried out on 50*50*50 mm cubic mould, whilst the flexural strength test was carried out with prism mould of 40*40*160 mm. Meanwhile, the direct tensile strength was examined on a dog-bone-shaped mould. Table 2 illustrates mix proportions of the mixtures. The samples were ambiently cured for 28 days before being tested. The number after the letter S is the percentage ratio of slag, the number after the letter P is the percentage ratio of pumice powder, and the last number for each mix is the s/b ratio.

2.3 Test Process

2.3.1 Setting Time

The setting time of AAM was evaluated through the Vicat apparatus (Sleiman, Perrot and Amziane 2010). In this test, the penetration of the 1 mm needle into the paste is measured. The initial setting time, according to ASTM C191-04b, is the elapsed time when the needle penetrates 25 mm from the contact moment between the binder and the solution from the surface of the paste. The time elapsed when no impression is left on the top surface of the paste after releasing the 5 mm needle is the final setting time. The temperature is set to room temperature. Four pastes with s/b values of 0.38, 0.4, 0.5 and 0.6 were examined, and the results of the setting time test were recorded. Figure 2 shows the Vicat apparatus with mortar under test.

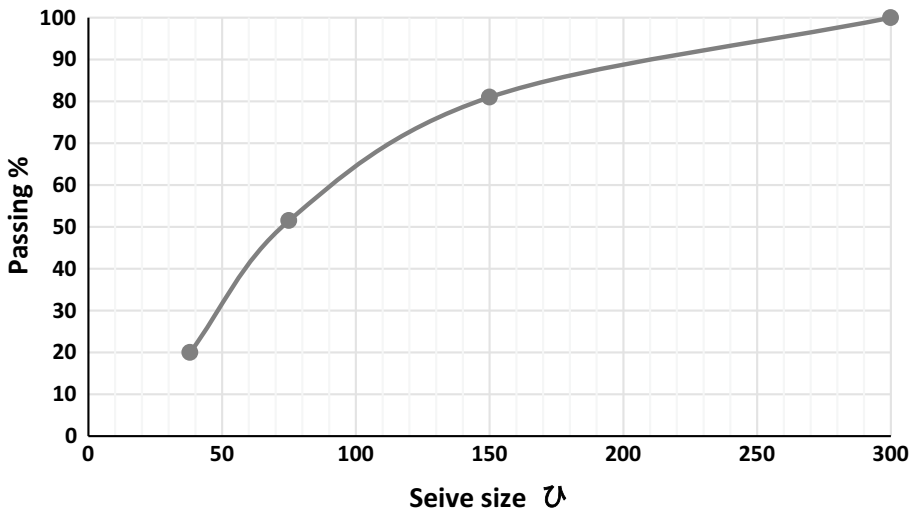

Fig. 1 Sieve analysis of pumice powder particles

Table 1 Chemical composition of both slag and pumice powder

Oxides	SiO_2	Al_2O_3	CaO	Fe_2O_3	MgO	SO_3	Na_2O	K_2O	BF (m^2/kg)	SpGr
Slag	28.17	8.572	47.75	0.414	3.805	1.452	0.021	0.295	419	2.78
Pumice powder	64.6	17.3	4.6	3.86	1.34	0.35	4.8	0.136	385	0.76

BF Specific surface area by Blaine method, *SpGr* Specific gravity

Table 2 Mix proportion of mixes

Mix code	Slag (g)	Pumice powder (g)	Sand (g)	Solution/ Binder (s/b)	Alkaline solution (g)	Superplasticiser (g)
S100P0-0.4	4750	0	4750	0.40	1900	95
S90P10-0.4	4275	475	4750	0.40	1900	95
S80P20-0.4	3800	950	4750	0.40	1900	95
S100P0-0.5	4750	0	4750	0.50	2375	95
S90P10-0.5	4275	475	4750	0.50	2375	95
S80P20-0.5	3800	950	4750	0.50	2375	95
S100P0-0.6	4750	0	4750	0.60	2850	95
S90P10-0.6	4275	475	4750	0.60	2850	95
S80P20-0.6	3800	950	4750	0.60	2850	95

Fig. 2 Vicat apparatus to determine the setting time of AAM

2.3.2 Flow Table Test

This test was performed according to BS 1881 part 105: 1984. The mould was filled with two layers and tamped 10 times with a wooden hammer within the cone. The mould was filled, the top was levelled, the cone was raised vertically, the table was raised 15 times, and the mean values of the two diameters were measured to determine the fluidity of the mixture. Figure 3 shows the devices under test.

2.3.3 Compressive Strength

The compressive strength of the samples was carried out using the ASTM standard (Standard 2008). A computerised compression machine with a maximum load carrying capability of 2000 kN was utilised as shown in Fig. 4. The average values of three cubic samples 50*50*50 mm were measured. The outcomes were noted at 7, 28 and 56 days old.

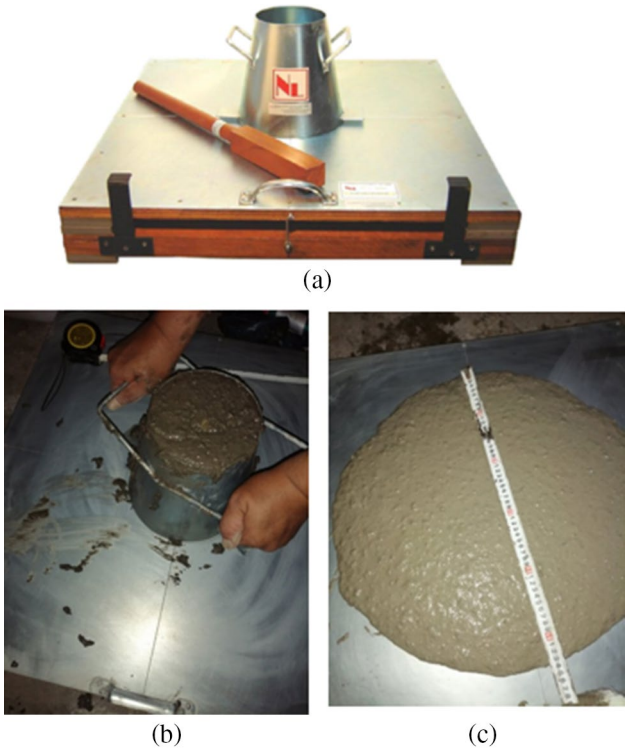

Fig. 3 Cone and table used to conduct flow table test and evaluate the flowability of the mixture: **a** flow table devices; **b** compacted fresh alkali-activated mortar inside the cone; **c** flowed alkali-activated mortar

2.3.4 Flexural Strength

This test was performed on 40*40*160 mm prism after 28 days of casting regarding ASTM C348 (ASTM C348-18 2018). A conventional three-point flexural test was used to assess the flexural strength of AAM specimens. The results of the flexural test were measured. Figure 5 shows the devices under test.

Fig. 4 Compression apparatus

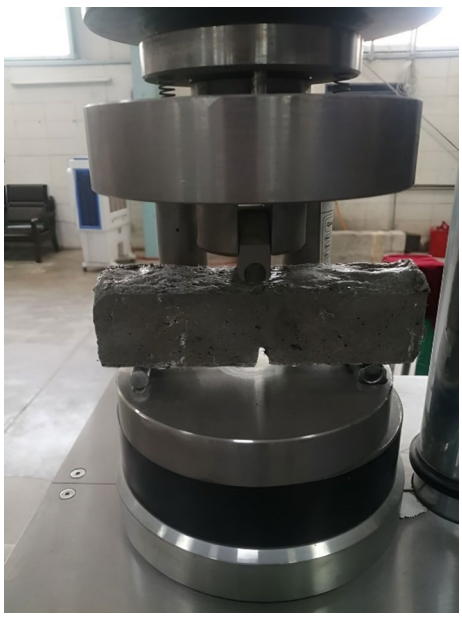

Fig. 5 Three-point flexural tensile strength machine

2.3.5 Direct Tensile Strength

The uniaxial tensile test was used to assess the direct tensile strength of AAM samples using the dog-bone-shaped samples recommended by the Japan Society of Civil Engineers. Figure 6 depicts the specimen's geometry and the specimen undergoing a direct tensile strength test. Three specimens were used for each mix. The samples were put under a quasi-static uniaxial tension.

2.3.6 Fire Resistance

This test was performed according to ISO 834. Three cubic samples 50*50*50 mm for each mix were heated for 2 h at 750 °C; 1000 °C and 1200 °C after 28 days of ambient curing. Afterwards, the samples were cooled to room temperature. The average value of the residual compressive strength was measured for samples of each mix. Figure 7 shows the samples still inside the oven.

2.3.7 Water Sorptivity

This test describes the water absorption of material from the bottom part of the samples by capillary action. It assesses the durability of the material. The ASTM C1585 standard was used to assess the water sorptivity of alkali-activated mortar (ASTM C1585 - 04E, 2004). For each mix, three cubic samples with a dimension of 50*50*50 mm were used to assess the AAM samples' water sorptivity. The samples were dried in an oven at 105 °C. Then, the samples were cooled to ambient temperature before being coated with a silicone strip to prevent water from seeping from the sides. They were then placed in water that was no deeper than 4 mm above the bottom of the sample. At various time intervals, the increase in mass was recorded and converted to the rising of water from the bottom as shown in Fig. 8.

2.3.8 Water Absorption

This test evaluates the durability of the material. It is expressed as the amount of water absorbed and retained by a material in a particular condition. The samples were first dried for 24 h at 110 °C in an oven. Thereafter, the samples were cooled to room temperature. Afterwards, the samples were kept in water for another 24 h. Water absorption was expressed as the percentage of increased mass from the oven-dry mass.

$$WA = \frac{(W2 - W1)}{W2} * 100 \quad (1)$$

where WA denotes water absorption, W1 and W2 are the oven-dry mass and saturated mass of the sample, respectively.

2.3.9 Density

To measure the density of the samples, the following procedure was considered. Firstly, the samples were dried for 24 h at 110 °C in an oven. After cooling the samples to room temperature, W1 was noted. Secondly, the samples were kept

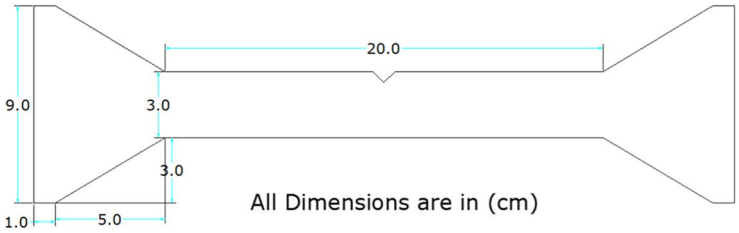

Fig. 6 Details of direct tensile strength sample and test

Fig. 7 Furnace with 1200 °C capacity to evaluate the fire resistance of AAM

in water for 24 h, and the W2 was recorded. Afterwards, the samples were submerged in water and weighed to obtain W3. The density was measured using the following formula:

$$Density = \frac{W1}{(W2 - W3)} \tag{2}$$

where W1 is the oven-dry mass, W2 is the saturated surface dry mass and W3 is the submerged mass.

2.3.10 Porosity

The permeability of a material increases as its porosity increases, indicating that high permeability results in a less durable material. In general, this process examines the accessible voids as well as the volume of the pores and voids. Reduced porosity specimens have higher compressive strength (Ameri et al. 2019).

To determine the porosity, the following procedure was considered. Firstly, the samples were dried for 24 h at 110 °C in an oven. After cooling the samples to room temperature, W1 was noted. Secondly, the samples were kept in water for 24 h, and the W2 was recorded. Afterwards, the samples were submerged in water and weighed to obtain W3. The density was measured in the following formula:

$$Porosity = \frac{(W2 - W1)}{(W2 - W3)} * 100 \tag{3}$$

where W1 is the oven-dry mass, W2 is the saturated surface dry mass and W3 is the submerged mass.

2.3.11 Efflorescence

This test was conducted on the samples according to Iraqi specification. The samples were put in a tray dish, and water was poured to a height of 25 mm. Absorbing or evaporating

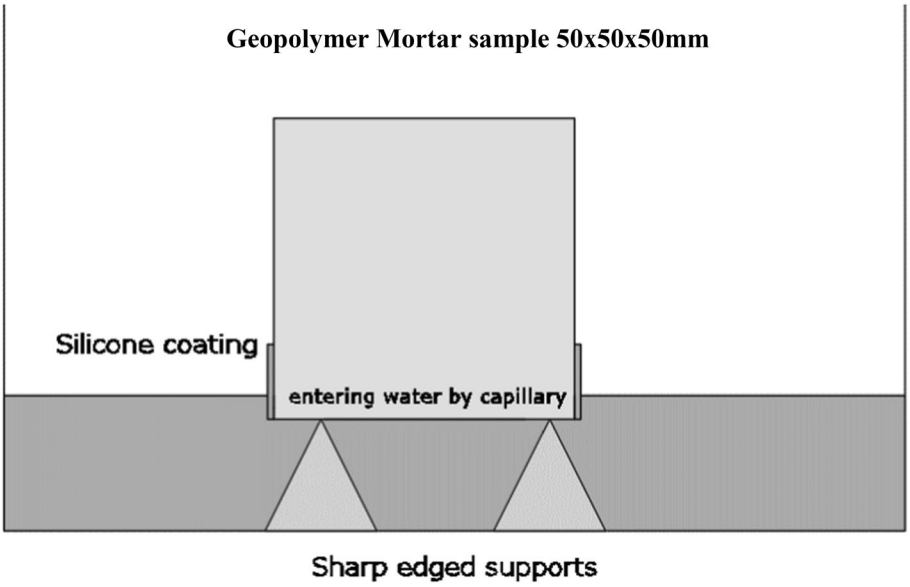

Fig. 8 Sorptivity test for AAM

the water requires seven days. Afterwards, water was poured again to the same height. After 3 days, the samples were dried, and a white deposit appeared on the sides of the samples. The efflorescence rate can be measured as follows:

$$Efflorescence\ rate = \frac{A1}{A2} * 100 \quad (4)$$

where A1 is the white deposit area in mm^2, and A2 is the total surface area of the samples in mm^2.

2.3.12 Sulphate Attack

To estimate the resistance of the AAM samples against sulphate attack, three samples from each mixture were kept in a 5% magnesium sulphate solution for one year as shown in Fig. 9. The samples were tested for visual appearance, compressive strength change and mass change compared with ambient-cured samples, and the results were noted.

Fig. 9 Specimens exposed to magnesium sulphate solution

3 Results and Discussion

3.1 Setting Time

Figure 10 shows the slag-based AAMs' setting time. According to the achieved results, the setting time and solution-to-binder ratio are correlated linearly. As the solution-to-binder ratio increased, the initial setting time was basically extended. The relationship between the setting time and solution-to-binder ratio is a straight line. The decreasing solution-to-binder ratio led to a reduction in the alkali-activated mortar's setting time. The mixes with higher solution-to-binder ratio have higher water content that led to a more fluid paste. Furthermore, it led to further needle penetration through the mixture. The mix needs extra time to consume the water through chemical actions or evaporation to be stiff.

3.2 Flow Table Test

Figure 11 depicts the effect of the addition of pumice powder and the solution binder ratio on the flowability of alkali-activated mortar. As the amount of pumice powder and the solution-to-binder ratio were changed, the mortar's flowability changed. Any increase in the amount of pumice powder reduced the flowability of the mortar for all ratios of solution to binder. This phenomenon was due to the fact that pumice powder has a porous nature, water tightness and greater specific surface area than slag. By contrast, raising the s/b from 0.40 to 0.60 improved flowability. The mixes with a

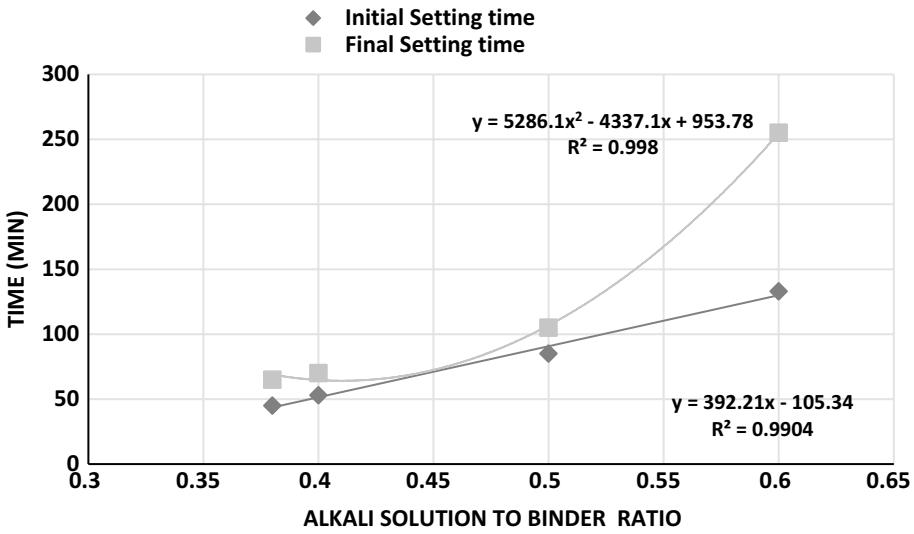

Fig. 10 Setting time of AAM

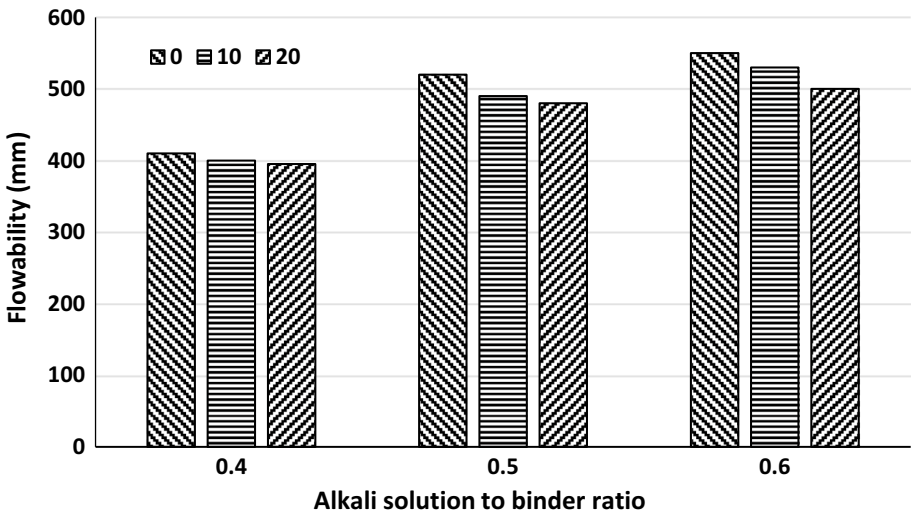

Fig. 11 Flowability of AAM with various pumice replacement and s/b ratios

higher solution-to-binder ratio have higher water content that led to a more fluid mix. Furthermore, it led to mixture with more flowability.

3.3 Compressive Strength

Figure 12 depicts the change in compressive strength at ages 7, 28 and 56 days with various solution-to-binder ratios and pumice powder replacements. Raising the s/b from 0.4 to 0.6 led to a decrease in the compressive strength because increasing the water content in the mixes after hardening led to an increase in the pores inside the samples; consequently, compressive strength decreased. Other researchers supported this finding (Chi 2017). Increasing the pumice powder content after 28 days at a s/b of 0.4 from 0 to 10% and 20% reduced the compressive strength from 33.51 MPa to 28.65 MPa and 27.76 MPa, respectively, as no appropriate alkali solution exists for the complete geopolymerisation process. Given that slag is more reactive at this phase, the alkaline solution may be completely absorbed in the condition of s/b = 0.4. By contrast, increasing the pumice powder content in the mixes improved the compressive strength at both s/b values of 0.5 and 0.6 probably owing to the existing alkali solution that would reactivate the pumice powders. The optimum s/b ratio for the slag-based AAM was 0.4. The results agree with those of other mechanical characteristics.

3.4 Flexural Strength

The flexural tensile strength of AAM changes, depending on the ratio of solution to binder and the amount of pumice powder as illustrated in Fig. 13. After 28 days, increasing the s/b from 0.4 to 0.6 led to a decrease in the flexural strength

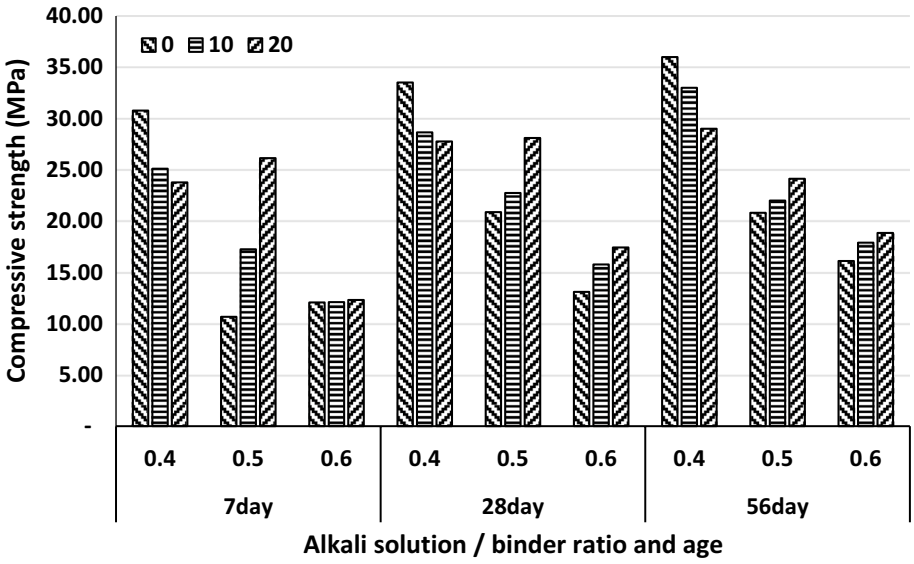

Fig. 12 Effect of both s/b ratio and different pumice powder contents on compressive strength

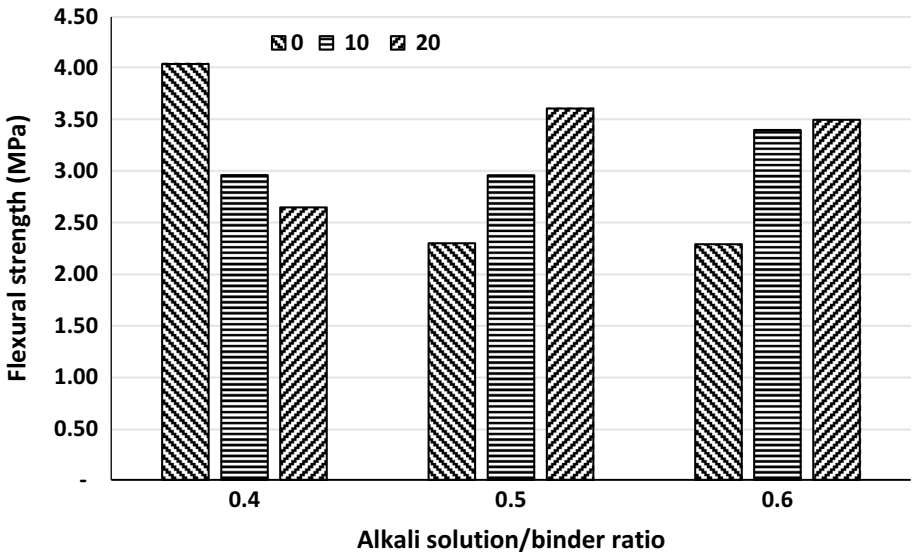

Fig. 13 Flexural strength of AAM with different s/b ratios and pumice powder replacement

because increasing the water content in the mixes after hardening led to an increase in the pores inside the samples. Consequently, flexural strength decreased. Other researchers supported this finding (Chi 2017). At a s/b of 0.4, increasing the pumice powder content from 0 to 10% and 20% decreased the flexural strength from 4.04 MPa to 2.96 MPa and 2.65 MPa, respectively, as no appropriate alkali solution exists for the complete geopolymerisation process. Given that slag is more reactive at this phase, the alkaline solution may be completely absorbed in the condition of s/b = 0.4. Adversely, at both s/b of 0.5 and 0.6, increasing the pumice powder content in the mixes improved the flexural strength probably due to the presence of an adequate alkali solution to reactivate the pumice powders. The optimum s/b ratio for the slag-based AAM was 0.4. The results are in good agreement with other mechanical characteristics.

3.5 Direct Tensile Strength

Figure 14 displays the variation of the direct tensile strength of alkali-activated mortar after 28 days with various s/b ratios and pumice powder substitution. Increasing the s/b from 0.4 to 0.6 led to a decrease in the direct tensile strength because increasing the water content in the mixes after hardening led to an increase in the pores inside the samples; consequently, direct tensile strength decreased. Other researchers supported this finding (Chi 2017). When the pumice powder content was increased from 0 to 10% and 20% at an s/b of 0.4, direct tensile strength fell from

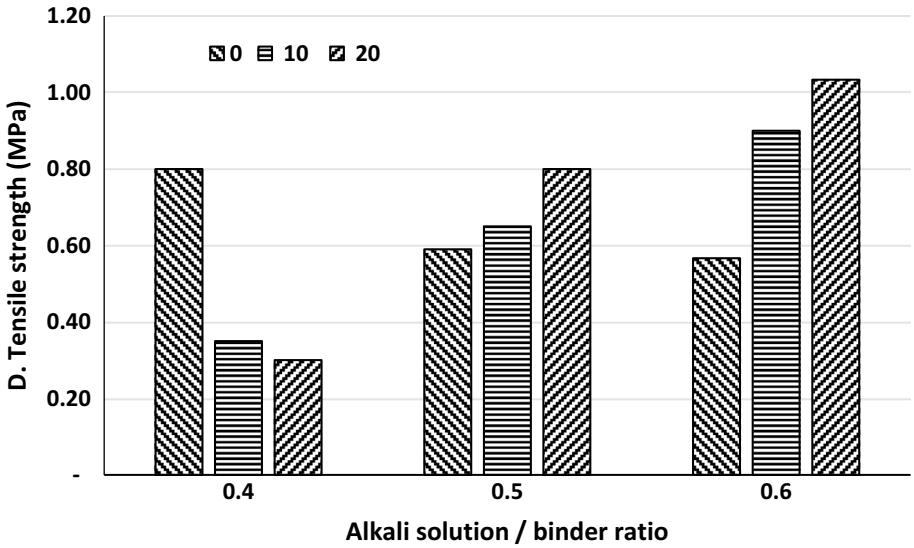

Fig. 14 Direct tensile strength of AAM with different s/b ratios and pumice powder

0.80 MPa to 0.35 MPa and 0.30 MPa, respectively as no appropriate alkali solution exists for the complete geopolymerisation process. Given that slag is more reactive at this phase, the alkaline solution may be completely absorbed in the condition of s/b = 0.4. Adversely, at both s/b of 0.5 and 0.6, increasing the pumice powder content in the mixes improved the direct tensile strength probably due to the presence of an adequate alkali solution to reactivate the pumice powders. The optimum s/b ratio for the slag-based AAM was 0.4. Similar results were shown for the compressive and flexural tensile strength.

3.6 Fire Resistance

Figure 15 indicates the residual compressive strength after exposing the samples to elevated temperatures of 750 °C; 1000 °C and 1200 °C. Generally, residual compressive strength after exposing to 1000 °C is higher than that of 750 °C and 1200 °C probably due to the densification of the mortar microstructure at this temperature. For all elevated temperatures and solution/binder ratios, increasing the pumice content improved residual strength. This finding might be due to the fact that the AAM includes pumice powder, which presents huge numbers of pores to reduce heat stress and improve the residual compressive strength. In addition, raising the s/b ratio improved the residual compressive strength of the alkali-activated mortar at elevated temperatures of 750 °C; 1000 °C and 1200 °C. Given that high s/b ratio, additional pores were present, which released thermal stress.

However, at s/b of 0.4 in both 1000 °C and 1200 °C, raising the pumice powder content deteriorated the residual

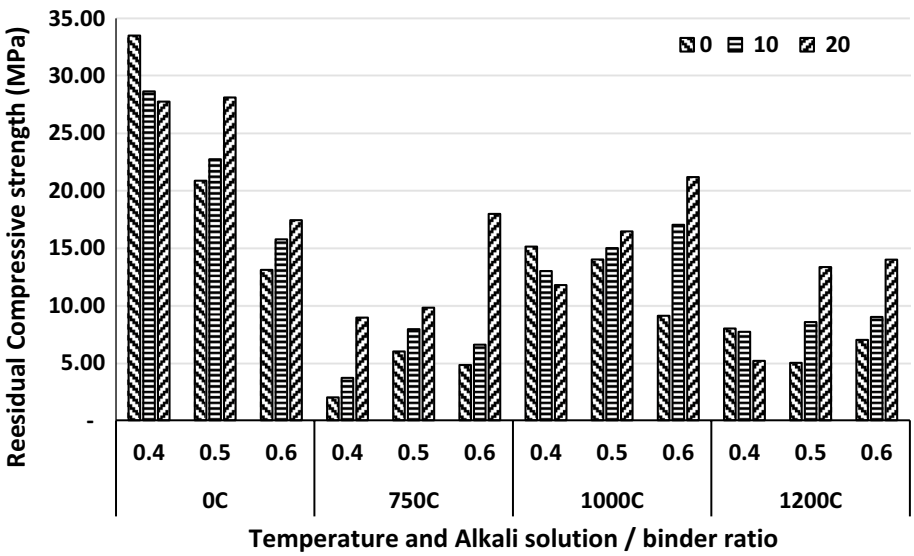

Fig. 15 Residual compressive strength of AAM with various s/b ratios and pumice powder replacement

compressive strength. This finding might be due to the fact that the geopolymerisation process did not complete and the pumice powder did not react completely with the alkaline solution to contribute to the strength of the mortar at this s/b ratio.

3.7 Water Sorptivity

Figure 16 shows the water sorptivity test results. Increasing the s/b from 0.4 to 0.6 led to an increase in the water sorptivity because increasing the water content in the mixes after hardening led to an increase in the pores inside the samples. Consequently, water sorptivity increased. An increase in the pumice powder content was also observed to cause the water sorptivity of AAM to rise at s/b = 0.4. The geopolymerisation and bonding process with other components was not completed when the s/b was 0.4 for AAM. Therefore, the sorptivity of AAM at a s/b ratio of 0.4 was increased with a rise in pumice powder content in the mixes. However, at both s/b ratios of 0.5 and 0.6, the addition of pumice powder decreased the water sorptivity. Meanwhile, the number and size of pores inside the AAM decreased due to the completion of the geopolymerisation process. This phenomenon also primarily explains why the mechanical characteristics of AAM were also influenced.

3.8 Water Absorption

Figure 17 shows the results of the water absorption test. Increasing the s/b from 0.4 to 0.6 led to an increase in the water absorption because increasing the water content in the mixes after hardening led to an increase in the pores inside the samples; consequently, water absorption increased (Chi 2017). At s/b 0.4, increasing the amount of pumice powder increased the water absorption. Meanwhile, the number and size of pores increased. The geopolymerisation and bonding process with other components were not completed when the s/b was 0.4 for AAM. Therefore, the water absorption of AAM at a s/b ratio of 0.4 was increased with a rise in the pumice powder content in the mixes which explains why the mechanical characteristics were also influenced. Moreover, at both s/b ratios of 0.5 and 0.6, the addition of pumice powder decreased the water absorption. Meanwhile, the number and size of

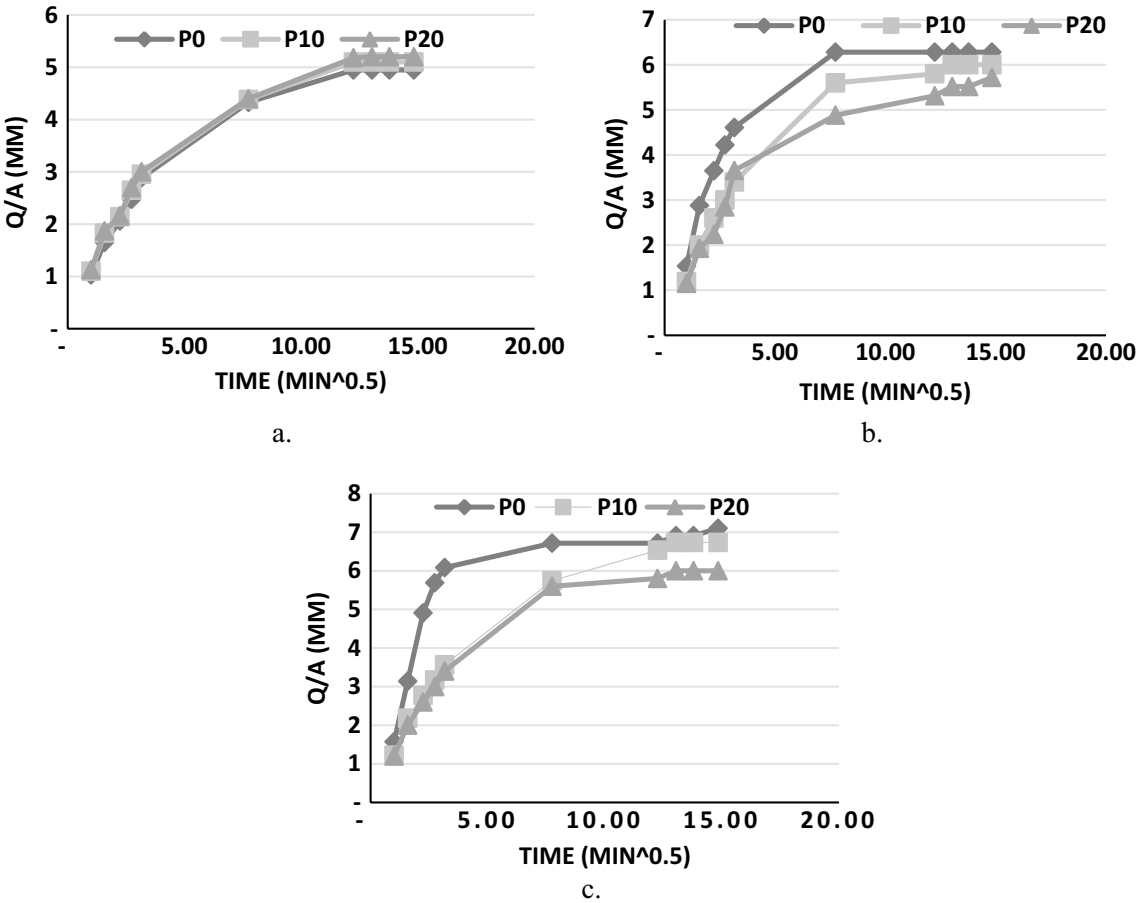

Fig. 16 Water Sorptivity of AAM with various s/b ratios and pumice powder replacement: **a** s/b = 0.4, **b** s/b = 0.5, **c** s/b = 0.6

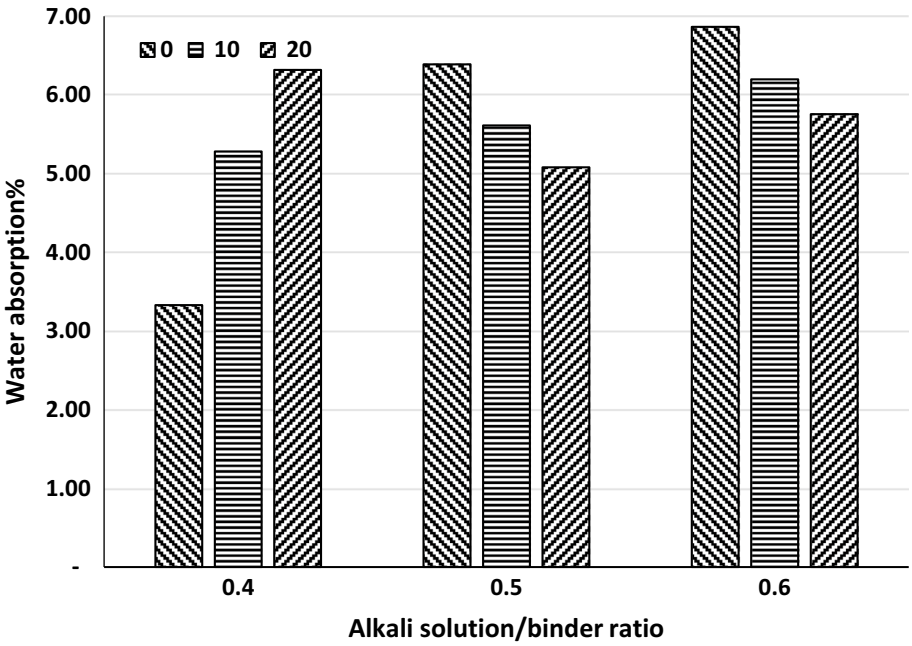

Fig. 17 Water absorption of AAM with a/b ratio and pumice powder replacement

pores inside the AAM decreased due to the completion of the geopolymerisation process.

3.9 Porosity

Figure 18 illustrates the porosity results of AAM. Increasing the s/b from 0.4 to 0.6 led to an increase in the porosity because increasing the water content in the mixes after hardening led to an increase in the pores inside the samples; consequently, porosity increased (Chi 2017). The porosity of AAM declined with the addition of pumice powder. At a s/b ratio of 0.4. The geopolymerisation and bonding process with other components were not completed when the s/b was 0.4 for AAM. By contrast, at both s/b of 0.5 and 0.6, the porosity was considerably decreased with the addition of pumice powder as a result of the complete geopolymerisation process and lower pore size.

3.10 Density

As seen in Fig. 19, the slag-based geopolymer mortar had a high density. Increasing the s/b from 0.4 to 0.6 led to a decrease in density because increasing the water content in the mixes after hardening led to an increase in the pores inside the samples. Consequently, density decreased. When the s/b is 0.4, adding pumice powder reduced the density by a small amount as the geopolymerisation and bonding process with other components were not completed when

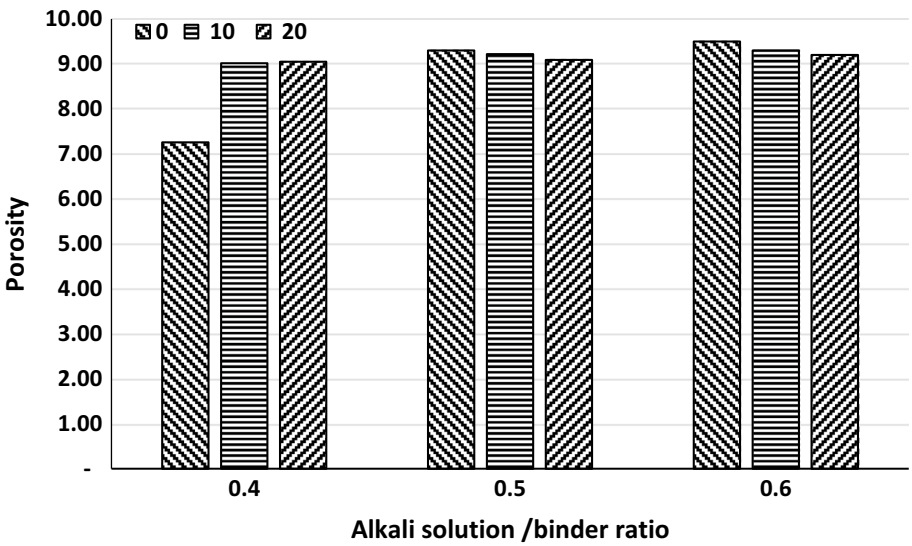

Fig. 18 Porosity of AAM with s/b ratio and pumice powder replacement

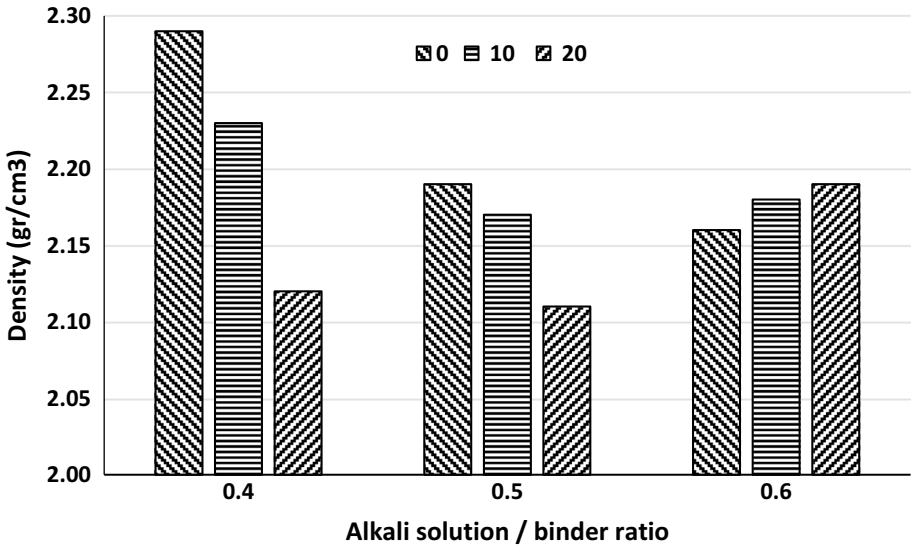

Fig. 19 Variation in density of AAM with different solution-to-binder ratios and pumice powder contents

the s/b was 0.4 for AAM. The density somewhat increased with increasing pumice powder concentration for both s/b values of 0.5 and 0.6 due to the complete geopolymerisation process and lower pore size.

3.11 Efflorescence

Figure 20 shows the efflorescence rate of AAM. Increasing the s/b from 0.4 to 0.6 increased the efflorescence because the water content in the mixes increased. After the samples were hardened, the pores inside the samples expanded. At a s/b of 0.4, the efflorescence reduced with an increase in the amounts of pumice powder. Notably, the inclusion of pumice powder considerably enhanced the efflorescence rate probably due to the fact that pumice powder had a filler effect. Furthermore, an increase in s/b resulted in a considerable increase in AAM efflorescence rate. The addition of pumice powder had a negative effect on the efflorescence ratio at both s/b ratios of 0.5 and 0.6; more efflorescence was seen at high s/b ratios and higher quantities of pumice powder. Some unreacted chemicals escaped to the surface of the samples as a result of the high accessible voids.

3.12 Sulphate Attack

3.12.1 Visual Appearance

Figure 21 shows the samples exposed to 5% magnesium sulphate solution for 1 year. Apart from a white deposit on the top of the samples (Fig. 22), microscopic fissures extended up to 1 cm into the samples' depth. As shown by SEM in Fig. 23, this finding indicates the presence of chemical reactions as seen in regular Portland cement concrete.

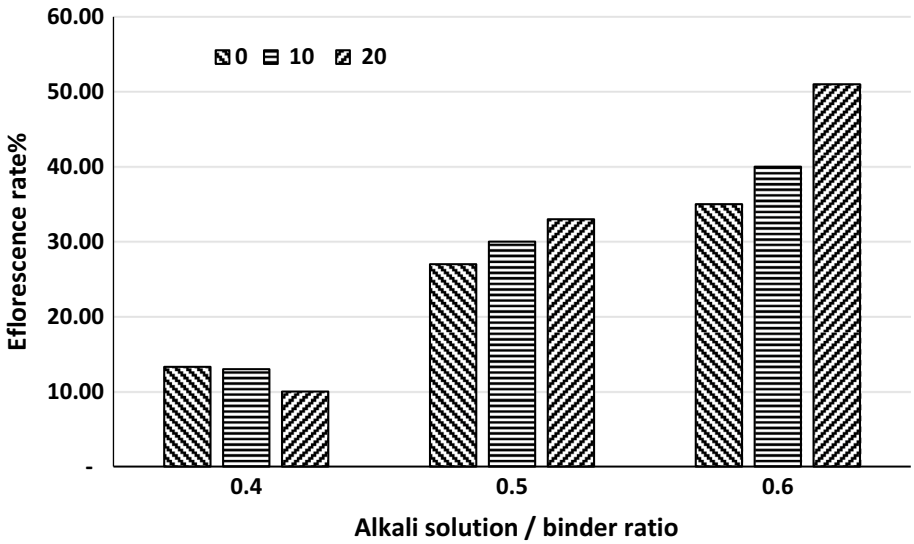

Fig. 20 Efflorescence rate of AAM with different s/b ratios and pumice powder replacement

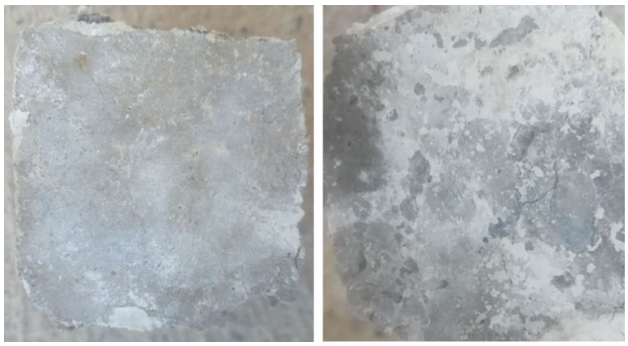

Fig. 21 Appearance of the AAM specimens exposed to 5% magnesium sulphate solution for 1 year

3.12.2 Mass Change

Figure 22 shows the change in mass after 12 months of immersing the samples in a 5% magnesium solution. Evidently, the mass loss of the samples increased when the solution/binder ratio increased from 0.4 to 0.5 and 0.6. Increasing the amount of pumice powder in the mixes simultaneously increased the mass loss. Increasing the pumice powder concentration from 0 to 10% and 20% resulted in 1.64, 1.77, and 1.80% mass losses, respectively, at s/b of 0.4. However, increasing the pumice powder concentration from 0 to 10% and 20% resulted in mass losses of 1.81, 1.89 and 1.91%, respectively, at s/b of 0.5. At s/b of 0.6, the mass losses from 0 to 10% and 20% pumice powder content were 1.92, 1.95, and 1.97%, respectively. Increasing the s/b led to an increase in porosity. Consequently, mass loss increased.

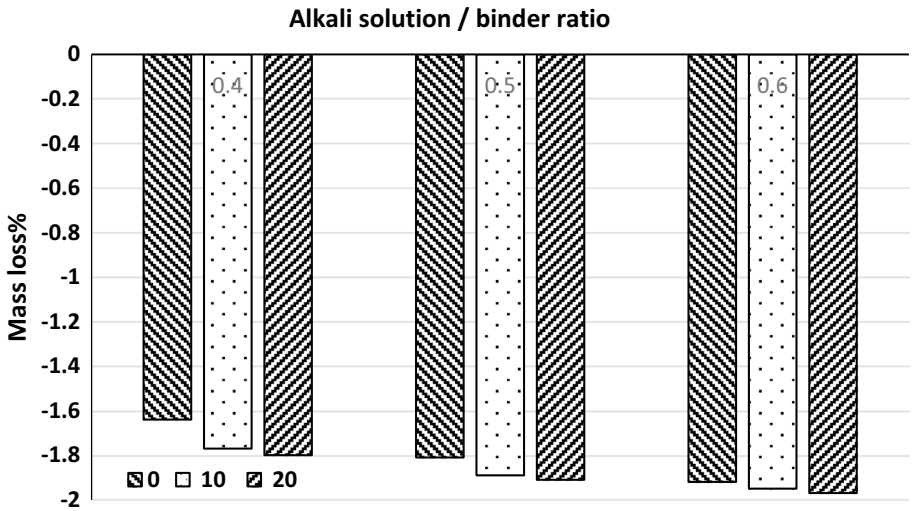

Fig. 22 Mass loss % for the specimens exposed to 5% magnesium sulphate solution

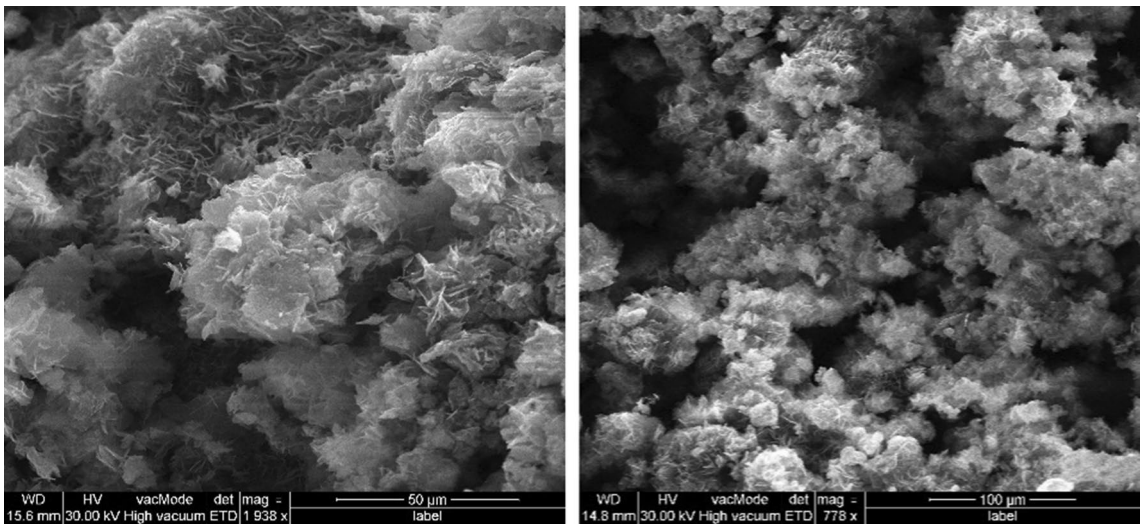

Fig. 23 SEM photo presents the white deposit up to 1 cm for the height of the specimen

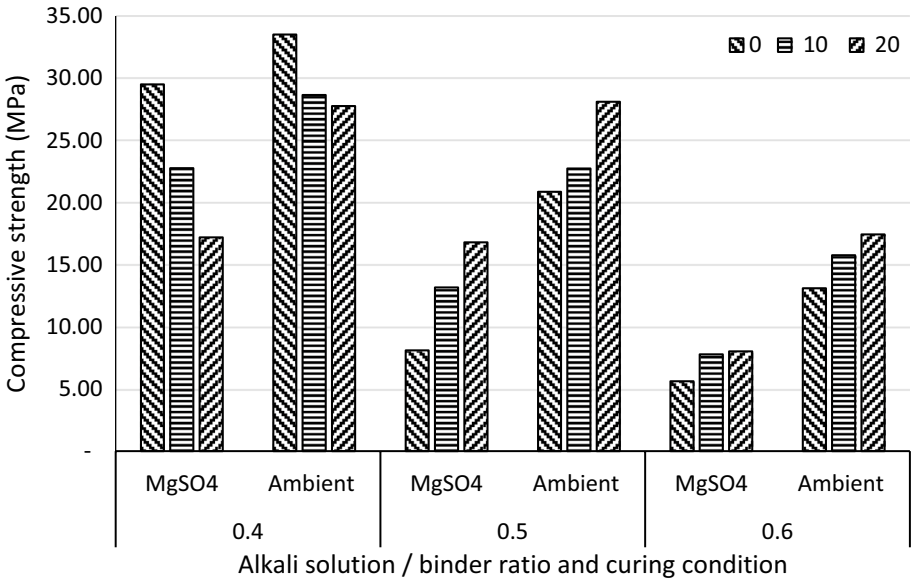

Fig. 24 Change in compressive strength for the specimens exposed to magnesium sulphate solution

By contrast, as the amount of pumice powder increased, the mass loss rose probably because of the AAM gel disintegration, causing a porous mass and structural damage. Other authors showed similar results (Guo et al. 2020).

3.12.3 Compressive Strength Change

As shown in Fig. 24, after the samples were placed in magnesium sulphate solution with a concentration of 5% for one year, a reduction in compressive strength was observed.

Obviously, compressive strength loss increased by increasing the solution binder ratio from 0.4 to 0.5 and 0.6. Given that increasing the water content in the mixes after hardening led to an increase in the pores inside the samples, compressive strength consequently decreased.

At s/b of 0.4, increasing the amount of pumice powder from 0 to 10% and 20% reduced compressive strengths from 29.5, 22.7 and 17.19, respectively. The geopolymerisation and bonding process with other components was not completed when the s/b was 0.4 for AAM. At both s/b of 0.5 and s/b of 0.6, increasing the pumice powder content from 0 to 10% and 20% increased the compressive strength by 8.11, 13.17 and 16.8 percent, 5.63, 7.79 and 8.02 percent, respectively, probably because of the adequate alkali solution to reactivate the pumice powders. Curing the samples in a severe chemical solution led to the AAM gel disintegration causing a porous mass and structural damage. Other authors concluded the same results (Guo et al. 2020).

4 Conclusion

This study investigated the combined effect of alkali solution-to-binder ratio and the pumice powder replacement on the hardened and fresh behaviour of the alkali-activated mortar. The following findings were summarised below:

- The setting times considerably extended with an increase in the alkali solution-to-binder ratio
- The flowability of the mixture increased considerably with an increase in the alkali-to-binder ratio despite adding superplasticiser. By contrast, the flowability of the mixture minimised with an increase in the amount of pumice powder.
- The mechanical properties (compressive strength, flexural tensile strength and direct tensile strength) improved as the pumice powder replacement increased for both s/b ratios (0.5 and 0.6). By contrast, with a s/b ratio of 0.4, the mechanical properties of the mixes decreased as the pumice powder replacement increased.
- The residual compressive strengths at 750 °C; 1000 °C and 1200 °C for all s/b ratios increased as the pumice powder replacement increased. Adversely, at (1000 °C and 1200 °C) with a s/b ratio of 0.4, increasing the pumice powder content decreased the residual compressive strength of the mixtures. The residual compressive strengths at 750 °C and 1200 °C were lower than the residual compressive strength at 1000 °C.
- The water sorptivity and water absorption at s/b of 0.4 were decreased with the pumice powder content. Adversely, at both s/b of 0.5 and 0.6, the water sorptivity and absorption increased along with an increase in the pumice powder content.
- The geopolymerisation process was completed with s/b 0.5 and 0.6, resulting in a substantial increase in the durability and mechanical performance of AAM.
- At a s/b of 0.4, increasing the amount of pumice powder resulted in a decrease in density and an increase in porosity. By contrast, increasing the pumice powder amounts resulted in an increase in density and a decrease in porosity for both s/b of 0.5 and 0.6.

- Increasing the pumice powder concentration resulted in lower efflorescence at a s/b of 0.4. Increasing the pumice powder content, in contrast to s/b values of 0.5 and 0.6, resulted in higher efflorescence. The efflorescence rate increased as the solution-to-binder ratio increased.
- AAM with a s/b = 0.4 and 0% pumice content showed excellent resistance to sulphate attack.

Declarations

Conflict of interest The authors declare that they have no competing interest.

References

Abdollahnejad Z, Luukkonen T, Mastali M, Kinnunen P, Illikainen M (2018) Development of one-part alkali-activated ceramic/slag binders containing recycled ceramic aggregates. J Mat Civ Eng 31(2):4018386

Aljanabi M, Çevik A, Nicş A, Bakbak D, Kadhim S (2022) Residual mechanical performance of lightweight fiber-reinforced geopolymer mortar composites incorporating expanded clay after elevated temperatures. J Com Mat 56(11):1737–1752

Allen G (2015) Hydraulic lime mortar for stone, brick and block Masonry: a best practice guide. Routledge, Oxfordshine

Al-Zboon KK, Al-smadi BM, Al-Khawaldh S (2016) Natural volcanic tuff-based geopolymer for Zn removal: adsorption isotherm, kinetic, and thermodynamic study. Water, Air, & Soil Poll 227(7):1–22

Alzeebaree R et al (2021) Using of recycled clay brick/fine soil to produce sodium hydroxide alkali activated mortars. Adv Stru Eng 24(13):2996

Ameri F, Shoaei P, Zareei SA, Behforouz B (2019) Geopolymers vs. alkali-activated materials (AAMs): a comparative study on durability, microstructure, and resistance to elevated temperatures of lightweight mortars. Con Buil Mat 222:49–63

Antoni A, Purwantoro AAT, Suyanto WSPD, Hardjito D (2020) Fresh and hardened properties of high calcium fly ash-based geopolymer matrix with high dosage of borax. Ira J Sci Tech, Tra Civ Eng 44(1):535–543

ASTM C1585 - 04E (2004) Standard test method for Measurement of rate of absorption of water by hydraulic-cement concretes. ASTM International, West Conshohocken, PA

ASTM C348 - 18 (2018) Standard test method for flexural strength of hydraulic-cement mortars standard test method for measurement the flaxural tensile strength of mortar

Bernal SA, Rodrguez ED, de Gutiérrez R, Provis JL (2012) Performance of alkali-activated slag mortars exposed to acids. J Sus Cem -Bas Mat 1(3):138–151

Bingöl SS, Bilim C, Atics CD, Durak U (2020) Durability properties of geopolymer mortars containing slag. Ira J Scie Tech, Tran Civ Eng 44(1):561–569

Chakkor O, Altan MF, Canpolat O (2022) Elevated temperature, freezing-thawing and mechanical properties of limestone, marble, and basalt powders reinforced metakaolin-red mud-based geopolymer mortars. Ira J Scie Tech Tran Civ Eng. https://doi.org/10.1007/s40996-021-00797-3

Chi M (2017) Effects of the alkaline solution/binder ratio and curing condition on the mechanical properties of alkali-activated fly ash mortars. Sci Eng Comp Mat 24(5):773–782

Clausi M, Fernández-Jiménez AM, Palomo A, Tarantino SC, Zema M (2018) Reuse of waste sandstone sludge via alkali activation in matrices of fly ash and metakaolin. Con Bui Mat 172:212–223

Davidovits J (1991) Geopolymers: inorganic polymeric new materials. J the Ana Calo 37(8):1633–1656

Davidovits J (2008) Geopolymer chemistry and applications (Geopolymer Institute, Saint-Quentin, France)

Degefu DM, Liao Z, Berardi U, Labbé G (2022) The effect of activator ratio on the thermal and hygric properties of aerated geopolymers. J Bu Eng 45:103414. https://doi.org/10.1016/J.JOBE.2021.103414

Djobo JNY, Elimbi A, Tchakouté HK, Kumar S (2016) Mechanical properties and durability of volcanic ash based geopolymer mortars. Con Buil Mat 124:606–614

Duxson P, Fernández-Jiménez A, Provis JL, Lukey GC, Palomo A, Van Deventer JSJ (2007) Geopolymer technology: the current state of the art. J Mat Sci 42(9):2917–2933. https://doi.org/10.1007/s10853-006-0637-z

El-Hassan H, Ismail N (2018) Effect of process parameters on the performance of fly ash/GGBS blended geopolymer composites. J Sust Cem -Bas Mat 7(2):122–140

Eren NA et al (2021) The effects of recycled tire rubbers and steel fibers on the performance of self-compacting alkali activated concrete. Per Poly Civ Eng. https://doi.org/10.3311/PPci.17601

Eren NA et al (2021) Fresh and hardened state performance of self-compacting slag based alkali activated concrete using nanosilica and steel fiber. J Com Mat. https://doi.org/10.1177/00219983211032390

Goldsworthy H, Zhu MIN (2009) Mortar studies towards the replication of Roman concrete. Arch 51(6):932–946

Guerrieri M, Sanjayan JG (2010) Behavior of combined fly ash/slag-based geopolymers when exposed to high temperatures. Fir Mat : an Inter Jo 34(4):163–175

Gülşan ME, Alzeebaree R, Rasheed AA, Niş A, Kurtoğlu AE (2019) Development of fly ash/slag based self-compacting geopolymer concrete using nano-silica and steel fiber. Con Bui Mat. https://doi.org/10.1016/j.conbuildmat.2019.03.228

Guo L, Wu Y, Xu F, Song X, Ye J, Duan P, Zhang Z (2020) Sulfate resistance of hybrid fiber reinforced metakaolin geopolymer composites. Com Part b: Eng 183:107689

Jha B, Singh DN (2011) A review on synthesis, characterization and industrial applications of flyash zeolites. J Ma Edu 33(1):65

Kabay N, Tufekci MM, Kizilkanat AB, Oktay D (2015) Properties of concrete with pumice powder and fly ash as cement replacement materials. Con Bui Mat 85:1–8

Kadhim S, Çevik A, Nicş A, Bakbak D, Aljanabi M (2022) Mechanical behavior of fiber reinforced slag-based geopolymer mortars incorporating artificial lightweight aggregate exposed to elevated temperatures. Con Bui Mat 315:125766

Kani EN, Allahverdi A, Provis JL (2012) Efflorescence control in geopolymer binders based on natural pozzolan. Cem Con Com 34(1):25–33

Kurtoğlu AE, Alzeebaree R, Aljumaili O, Niş A, Gülşan ME, Humur G, Çevik A (2018) Mechanical and durability properties of fly ash and slag based geopolymer concrete. Adv Con Con. https://doi.org/10.12989/acc.2018.6.4.345

Kurtoglu AE, Cevik A, Farhan OH, Alzeebaree R, Gülşan ME (2017) Sea water resistance of fly ash- and slag-based geopolymer concrete in Con: 2nd Inter Ene & Eng Con At: Gaziantep University, Gaziantep, Turkey, pp 273–279

Kwek SY, Awang H, Cheah CB (2021) Influence of liquid-to-solid and alkaline activator (sodium silicate to sodium hydroxide) ratios on fresh and hardened properties of alkali-activated palm oil fuel ash geopolymer. Mat 14(15):4253

Mahdi SN, Hossiney N, Abdullah MMAB (2022) Strength and durability properties of geopolymer paver blocks made with fly ash and brick kiln rice husk ash. Cas Stu Con Mat 16:e00800

Mason BJ (2012) The analysis of taupo pumice as an effective partial cement replacement in concrete

Mawlod AO (2020) Performance of one-part alkali activated recycled ceramic tile/fine soil binders. Adv Con Con 10(4):311–317

Mobasher N, Bernal SA, Provis JL (2016) Structural evolution of an alkali sulfate activated slag cement. J Nuc Mat 468:97–104

Mohamed R, Abd Razak R, Mustafa Al Bakri Abdullah M, Khimi Shuib R, Aida Mohd Mortar N, Wazien Ahmad Zailani W (2019) Investigation of heat released during geopolymerization with fly ash based geopolymer. IOP Conf Series: Mater Sci Eng 551:012093. https://doi.org/10.1088/1757-899X/551/1/012093

Nath P, Sarker PK (2015) Use of OPC to improve setting and early strength properties of low calcium fly ash geopolymer concrete cured at room temperature. Cem Con Com 55:205–214

Nesbitt HW, Young GM (1984) Prediction of some weathering trends of plutonic and volcanic rocks based on thermodynamic and kinetic considerations. Geo Cos Acta 48(7):1523–1534

Nis A, Eren NA, Çevik A (2021) Effects of nanosilica and steel fibers on the impact resistance of slag based self-compacting alkali-activated concrete. Cer Inter 47(17):23905–23918

Noushini A, Babaee M, Castel A (2016) Suitability of heat-cured low-calcium fly ash-based geopolymer concrete for precast applications. Mag Con Res 68(4):163–177

Pouhet R (2015) Formulation and durability of metakaolin-based geopolymers. Univ Toul III-Paul Sabatier, Uni Tou

Provis JL (2018) Alkali-activated binders. Cem Concr Res 114(40):48

Provis JL, Bernal SA (2014) Geopolymers and related alkali-activated materials. Ann l Rev Mat Res 44:299–327

Shi C, Day RL (1993) Chemical activation of blended cements made with lime and natural pozzolans. Cem Concr Rese 23(6):1389–1396

Sleiman H, Perrot A, Amziane S (2010) A new look at the measurement of cementitious paste setting by Vicat test. Cem Concr Res 40(5):681–686

Standard A (2008) ASTM C109-standard test method for compressive strength of hydraulic cement mortars ASTM Inte , West Conshohocken, PA

Tekin I (2016) Properties of NaOH activated geopolymer with marble, travertine and volcanic tuff wastes. Con Bui Mat 127:607–617

van Deventer JSJ (2015) Microstructure and durability of alkali-activated materials as key parameters for standardization. J Sus Cem-Bas Mat 4(2):116–128

Walkley B, San Nicolas R, Bernal S, Provis JL, van Deventer J (2015) Effect of MgO incorporation on the structure of synthetic alkali-activated calcium aluminosilicate binders in Conf. 27th Bienn. Natl. Conf. Concr. Inst. Aust

Winnefeld FB, Haha M, Le Saout G, Costoya M, Ko S-C, Lothenbach B (2015) Influence of slag composition on the hydration of alkali-activated slags. J Sus Cem-Bas Mat 4(2):85–100

Xinyan W, Yanghai S, Liang H (2022) Performance of geopolymer concrete activated by sodium silicate and silica fume activator. Cas Stu Con Mat 17:e01513

Yang T et al (2012) Mechanical property and structure of alkali-activated fly ash and slag blends. J Sus Cem-Bas Mat 1(4):167–178

Zamanabadi SN, Zareei SA, Shoaei P, Ameri F (2019) Ambient-cured alkali-activated slag paste incorporating micro-silica as repair material: effects of alkali activator solution on physical and mechanical properties. Con Buil Mat 229:116911

Zhao F-Q, Ni W, Wang H-J, Liu H-J (2007) Activated fly ash/slag blended cement. Reso, Conse Recy 52(2):303–313